

**All-atom Molecular Dynamics Simulations of Weak Polyionic Brushes:
Influence of Charge Density on the Properties of Polyelectrolyte Chains,
Brush-Supported Counterions and Water Molecules: Supplementary
Material**

Harnoor Singh Sachar,¹ Turash Haque Pial,¹ Bhargav Sai Chava,¹ and Siddhartha Das^{1*}

¹Department of Mechanical Engineering, University of Maryland,
4298 Campus Drive, College Park, MD 20742

*Email: sidd@umd.edu

S1. Relationship between pH and Degree of Ionization

Arnold et al¹ suggested the following fit between the degree of ionization (f) and pH for aqueous PAA solutions:

$$pH = pK_0 + mf^{1/3} - \log\left(\frac{1-f}{f}\right) \quad [S1]$$

where m is a constant and pK_0 is the negative logarithm of the dissociation constant of an isolated ($f \rightarrow 0$) ionizable group. We take the values $m=3.55$ and $pK_0=3.82$ for the highest PAA concentration probed in their work (0.0174 N). These values of m and pK_0 were fitted for salt-free solutions, which is consistent with our simulations. However, we must point out that our polyelectrolyte concentrations (~ 12 N) are orders of magnitude greater than their work because of high grafting density of the brushes. Moreover, their data was fitted for polyelectrolytes in solution and not for polyelectrolyte brushes. The confinement created by PE brushes can significantly alter the titration curve.

The following table shows the pH values (calculated using equation S1) at the various degrees of ionizations (f) studied in this paper. pH values corresponding to no ionization ($f=0$) and full ionization ($f=1$) were obtained by plugging $f=0.01$ and $f=0.99$ respectively in equation 1 (due to the singularity at $f=0, 1$).

f	0	0.25	0.5	0.75	1
pH	2.6	5.6	6.6	7.5	9.4

Table S1: pH values corresponding to the various degrees of ionization probed in our study

S2. MD Force Field parameters

In Figure S1, we provide a schematic representation of a partially ionized polyacrylic acid (PAA) molecule.

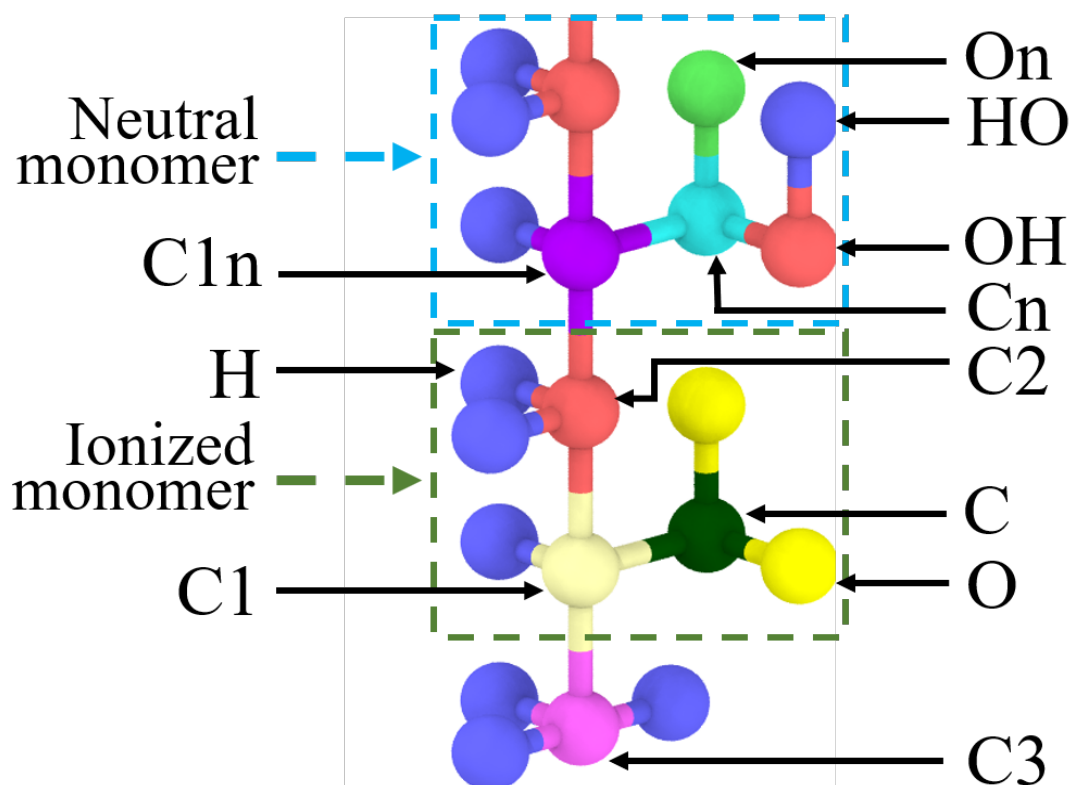


Figure S1: Schematic representation (not to scale) of a partially ionized polyacrylic acid (PAA) molecule. The arrows depict the atom types of their respective atoms. Dashed boxes indicate two different types of repeating units.

Non-bonded Potentials and Associated Parameters

The Coulombic pairwise interactions (U_{Coul}) between charged atoms are given by:

$$U_{Coul} = \frac{q_i q_j}{4\pi\epsilon_0\epsilon_1 r_{ij}}. \quad [S2]$$

and the 12-6 Lennard-Jones (LJ) potential (U_{LJ}) used in the simulations can be represented as:

$$U_{LJ} = 4\epsilon_{ij} \left[\left(\frac{\sigma_{ij}}{r_{ij}} \right)^{12} - \left(\frac{\sigma_{ij}}{r_{ij}} \right)^6 \right], \quad [S3]$$

In the above equations, q_i and q_j are the charges on i^{th} and j^{th} atoms respectively, r_{ij} is the Euclidian distance between atoms i and j , ϵ_0 is the permittivity of free space (vacuum), ϵ_1 is the relative permittivity of the background (equal to 1), ϵ_{ij} is the well depth for LJ interactions between atoms i and j and σ_{ij} is the distance corresponding to zero LJ potential between atoms i and j .

The values of these parameters for the various atom types shown in Figure S1 along with water and mobile ions are listed below in Table S2.

Atom Type	Charge (e)	Mass (amu)	ϵ (Kcal/mole)	σ (Å)
C3 (CH ₃)	-0.18	12.011	0.066	3.50
C2 (CH ₂)	-0.12	12.011	0.066	3.50
C1 (CH, Attached to COO ⁻)	-0.16	12.011	0.066	3.50
C (COO ⁻)	0.70	12.011	0.105	3.75
C1n (CH, Attached to COOH)	-0.06	12.011	0.066	3.50
Cn (COOH)	0.52	12.011	0.105	3.75
H	0.06	1.008	0.03	2.50
HO (H in COOH)	0.45	1.008	0.00	0.00
O (COO ⁻)	-0.80	15.999	0.210	2.96
On (O, Attached to C in COOH)	-0.44	15.999	0.210	2.96
OH (O, Attached to C and H in COOH)	-0.53	15.999	0.170	3.00
O _w (H ₂ O)	-0.8476	15.999	0.155354	3.166
H _w (H ₂ O)	0.4238	1.008	0	0
Na	1.00	22.99	0.3526418	2.1595
Continuous LJ Wall (Parameters remain unchanged for interaction with all atom types)	0.00	15.00794	0.1947	3.00 (LJ cut off length is 3.36 Å)

Table S2: Charge, mass and LJ parameters for various atom types

Bonded Potentials and Associated Parameters

The potential energy for bonds is considered in harmonic form, which is expressed as:

$$U_{bond} = K_b(r - r_0)^2, \quad [S4]$$

where r_0 is the equilibrium bond length and K_b is bond stiffness. The values of r_0 and K_b for different bond types are summarized below in Table S3.

Bond Type	$K_b, \left(\frac{\text{Kcal}}{\text{mol} \cdot \text{\AA}^2}\right)$	$r_0, (\text{\AA})$
C2-H	340.0	1.09
C2-C1	268.0	1.529
C1-H	340.0	1.09
C3-H	340.0	1.09
C-C1	317.0	1.522
C1-C3	268.0	1.529
C-O	656.0	1.25
C1n-H	340.0	1.09
C1n-C2	268.0	1.529
C1n-Cn	317.0	1.522
Cn-On	570.0	1.229
Cn-OH	450.0	1.364
OH-HO	553.0	0.945
C1n-C3	268.0	1.529
O _w -H _w	-	1.00

Table S3: Bond parameters for all different types of bonds

The potential energy for the angles between different bonds is considered in harmonic form and expressed as:

$$U_{angle} = K_a(\theta - \theta_0)^2, \text{ [S5]}$$

where θ_0 is the equilibrium angle value and K_a is the angle stiffness. The values of θ_0 and K_a for different angle types are listed in Table S4.

Angle Type	$K_a, (\frac{Kcal}{mol.rad^2})$	$\theta_0(deg)$
H-C2-H	33.00	107.8
H-C2-C1	37.5	110.7
C2-C1-H	37.5	110.7
C1-C3-H	37.5	110.7
H-C3-H	33.00	107.8
H-C1-C	35.0	109.5
O-C-O	80.0	126.00
C2-C1-C	63.0	111.1
C3-C1-C	63.0	111.1
H _w -O _w -H _w	-	109.47
C2-C1-C2	58.35	112.7
C2-C1-C3	58.35	112.7
C1-C-O	70.0	117.0
C3-C1-H	37.5	110.7
C1-C2-C1	58.35	112.7
C3-C1n-C2	58.35	112.7

H-C3-C1n	37.5	110.7
H-C1n-Cn	35.0	109.5
C2-C1n-C2	58.35	112.7
H-C2-C1n	37.5	110.7
C2-C1n-Cn	63.0	111.1
C1n-C2-C1n	58.35	112.7
C1n-Cn-On	80.0	120.4
C1n-Cn-OH	70.0	108.0
On-Cn-OH	80.0	121.0
Cn-OH-HO	35.0	113.0
C1-C2-C1n	58.35	112.7
C3-C1n-H	37.5	110.7
C3-C1n-Cn	63.0	111.1
H-C1n-C2	37.5	110.7

Table S4: Angle parameters for all different types of angles

The potential energy corresponding to proper dihedral interactions is expressed as:

$$U_{dihedral} =$$

$$\frac{1}{2}K_1[1 + \cos(\phi)] + \frac{1}{2}K_2[1 - \cos(2\phi)] + \frac{1}{2}K_3[1 + \cos(3\phi)] + \frac{1}{2}K_4[1 - \cos(4\phi)],$$

[S6]

where K_1 , K_2 , K_3 and K_4 are the Fourier coefficients associated with torsional interactions, and ϕ is the value of the torsional angle. Values of K_1 , K_2 , K_3 and K_4 are listed in Table S5.

Dihedral type	K_1 , (Kcal/ mole)	K_2 , (Kcal/ mole)	K_3 , (Kcal/ mole)	K_4 , (Kcal/ mole)
H-C2-C1-H	0.0	0.0	0.30	0.0
H-C2-C1-C	0.0	0.0	-0.10	0.0
H-C2-C1-C2	0.0	0.0	0.30	0.0
H-C2-C1-C3	0.0	0.0	0.30	0.0
H-C1-C-O	0.0	0.0	0.00	0.0
H-C1-C3-H	0.0	0.0	0.30	0.0
C2-C1-C-O	0.0	0.82	0.00	0.0
C2-C1-C2-C1	1.30	-0.05	0.20	0.0
H-C3-C1-C2	0.0	0.0	0.30	0.0
C3-C1-C-O	0.0	0.82	0.0	0.0
C1-C2-C1-C	-3.185	-0.825	0.493	0.0
C1-C2-C1-C3	1.30	-0.05	0.20	0.0
H-C1-C2-C1	0.0	0.0	0.30	0.0
H-C3-C1-C	0.0	0.0	-0.10	0.0

On-Cn-OH-HO	0.0	5.50	0.0	0.0
C1n-Cn-OH-HO	1.50	5.50	0.0	0.0
H-C1n-Cn-OH	0.0	0.0	0.0	0.0
C2-C1n-Cn-OH	1.0	0.546	0.45	0.0
C3-C1n-Cn-OH	1.0	0.546	0.45	0.0
H-C1n-Cn-On	0.0	0.0	0.00	0.0
C2-C1n-Cn-On	0.0	0.546	0.0	0.0
C3-C1n-Cn-On	0.0	0.546	0.0	0.0
H-C2-C1n-Cn	0.0	0.0	-0.10	0.0
C1-C2-C1n-Cn	-3.185	-0.825	0.493	0.0
C1n-C2-C1n-Cn	-3.185	-0.825	0.493	0.0
H-C3-C1n-Cn	0.0	0.0	-0.10	0.0
H-C1-C2-C1n	0.0	0.0	0.30	0.0
C1n-C2-C1-C	-3.185	-0.825	0.493	0.0
C1n-C2-C1-C2	1.30	-0.05	0.20	0.0
H-C1n-C2-C1n	0.0	0.0	0.30	0.0
C1n-C2-C1n-C2	1.30	-0.05	0.20	0.0
C1n-C2-C1-C3	1.30	-0.05	0.20	0.0
C1n-C2-C1n-C3	1.30	-0.05	0.20	0.0
H-C1n-C2-H	0.0	0.0	0.30	0.0
H-C1n-C2-H	0.0	0.0	0.30	0.0
H-C1n-C3-H	0.0	0.0	0.30	0.0
C2-C1n-C2-H	0.0	0.0	0.30	0.0

C2-C1n-C2-C1	1.30	-0.05	0.20	0.0
C3-C1n-C2-C1	1.30	-0.05	0.20	0.0
C3-C1n-C2-H	0.0	0.0	0.30	0.0
C2-C1n-C3-H	0.0	0.0	0.30	0.0

Table S5: Dihedral parameters for different types of dihedrals

Improper torsional dihedrals are considered in the harmonic form and expressed as:

$$U_{improper} = K_i(\varphi - \varphi_0)^2, [S7]$$

where φ_0 is the equilibrium improper torsional angle value and K_i is the associated improper torsional stiffness. The values of the improper dihedral parameters are listed below in Table S6.

Improper Type	$K_i \left(\frac{\text{Kcal}}{\text{mol.rad}^2} \right)$	$\varphi_0(\text{deg})$
C1-O-C-O	10.5	180
C1n-On-Cn-OH	10.5	180

Table S6: Improper dihedral parameters for different types of improper dihedrals

S3. Autocorrelation Function for Average End-point Brush Height

The autocorrelation function corresponding to the average end-point brush height was monitored throughout the simulations to check for convergence. The autocorrelation function for a given variable Z can be expressed as:

$$C_Z(t) = \frac{\langle (Z(t) - \langle Z \rangle)(Z(0) - \langle Z \rangle) \rangle}{\langle Z^2 \rangle - \langle Z \rangle^2},$$

where the angular brackets denote time average and $\langle Z \rangle$ is the mean value of variable Z over the sampling interval. Figure S2 plots the autocorrelation function for the average end-point height of the brushes [$C_e(t)$].

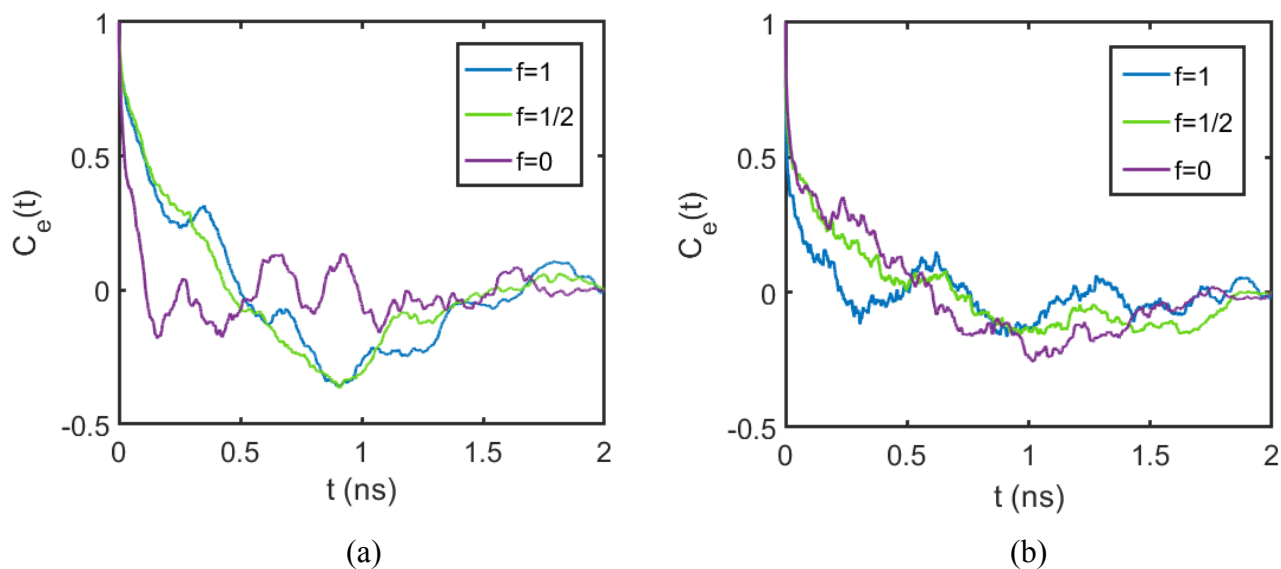


Figure S2: Autocorrelation function [$C_e(t)$] corresponding to the average end-point brush height, plotted over the production run for various degrees of ionization for (a) $\sigma_g = 0.1/\sigma^2$ and (b) $\sigma_g = 0.2/\sigma^2$. Only three values of degree of ionization (f) are plotted to avoid clutter.

The time scale corresponding to the autocorrelation function (τ_e) was calculated as:

$$\tau_e = \int_0^{t_0} C_e(t) dt / (1 - C_e(t_0)),$$

where t_0 is the time when $C_e(t) = 1/e^2$.

Table S7 lists the equilibration time (t_{equi}), production run time (t_{prod}) and the autocorrelation timescale (τ_e) for all simulations.

$\sigma_g^2 (1/\sigma^2)$	f	t_{equi} (ns)	t_{prod} (ns)	τ_e (ps)
0.1	0	14	2	42.37
0.1	0.25	16	2	137.07
0.1	0.5	16	2	158.19
0.1	0.75	12	2	44.76
0.1	1	12	2	136.92
0.2	0	10	2	54.38
0.2	0.25	10	2	12.94
0.2	0.5	8	2	72.60
0.2	0.75	6	2	7.06
0.2	1	8	2	13.44

Table S7: Equilibration time (t_{equi}), production run time (t_{prod}) and autocorrelation time scale (τ_e) for various degrees of ionization and grafting densities.

S4. Comparison of Brush Height with Scaling Laws

In this section, we compare our equilibrium end-point brush height with the scaling predictions of the non-linear osmotic brush regime³⁻⁵ and that of uncharged polymer brushes⁶. In this regime, the brush height is dictated by a balance between the elastic energy of the brushes and the entropy of the counterions. However, contrary to the osmotic brush regime, the counterion entropy in non-linear osmotic brush regime is calculated after removing the volume occupied by the PE chains (along with the condensed counterions).

The brush height for the non-linear osmotic brush regime is given by:

$$H_{osm, nl} = nb \frac{f + \sigma_{eff}^2 \sigma_g}{1 + f},$$

Here, $n=(N-1)/2$ is the number of repeating units (neutral or ionized) where N is the total number of backbone Carbon atoms, $b=3.058 \text{ \AA}$ is equal to 2 C-C bond lengths, f is the degree of ionization, σ_g is the grafting density and $\sigma_{eff} = \sqrt{2}\sigma$ is the effective monomer diameter after considering the volume of the condensed counterions.

The brush height for uncharged polymer brushes is given by:

$$H_{PB} = n \left(\frac{2w\sigma_g b^2}{3} \right)^{1/3},$$

Where w is the excluded volume parameter. Here we assume $w \approx b^3$, since water is a good solvent for the PAA brushes at all degrees of ionization.

Figure S3 compares the end-point brush heights obtained by MD simulations, the scaling laws of the non-linear osmotic brush regime and the scaling laws of uncharged polymer brushes for various degrees of ionization and grafting densities.

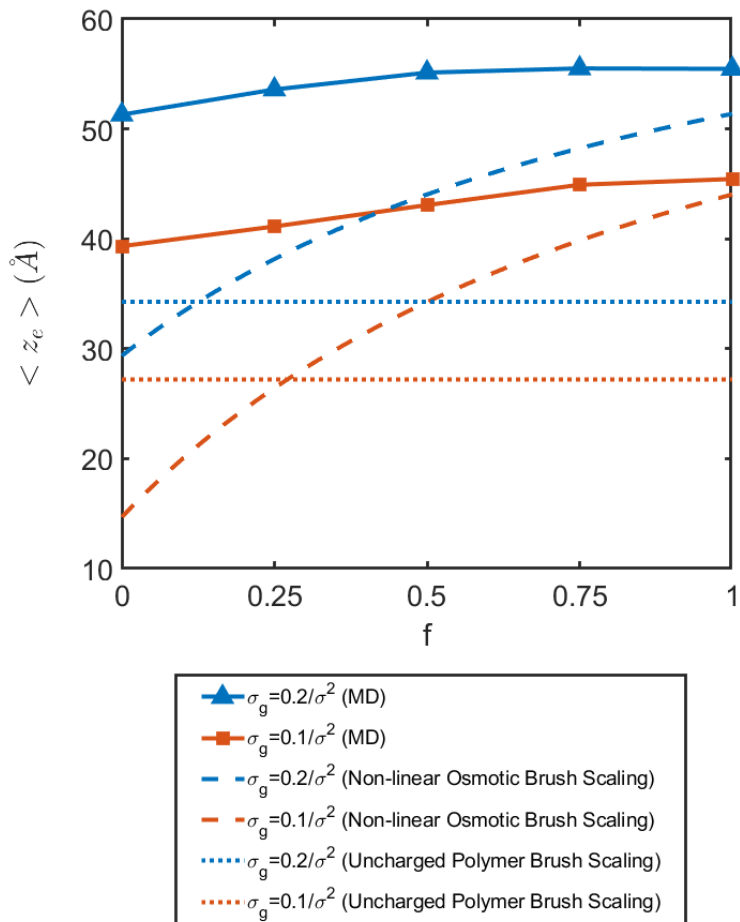


Figure S3: Equilibrium end-point brush height for different degrees of ionization and grafting densities obtained via MD simulations, scaling laws of the non-linear osmotic brush regime, and scaling laws of uncharged polymer brushes.

Table S8 lists the equilibrium end-point brush height obtained via MD simulations for all degrees of ionization and grafting densities.

$\sigma_g (1/\sigma^2)$	f	$\langle z_e \rangle (\text{\AA})$
0.1	0	39.33
0.1	0.25	41.12
0.1	0.5	43.07
0.1	0.75	44.92
0.1	1	45.44
0.2	0	51.30
0.2	0.25	53.59
0.2	0.5	55.12
0.2	0.75	55.50
0.2	1	55.46

Table S8: Equilibrium end-point brush height for various degrees of ionization and grafting densities.

S5. Mean Squared Displacement (MSD) of Backbone Carbon Atoms

Figures S4 (a) and (c) plot the mean squared displacement (MSD) of backbone Carbon atoms of the PE chains at $t=50$ ps for different degrees of ionization and grafting densities. In addition, Figures S4 (b) and (d) depict the MSD of the middle backbone Carbon atom (25^{th} Carbon atom) along each chain for different degrees of ionization and grafting densities.

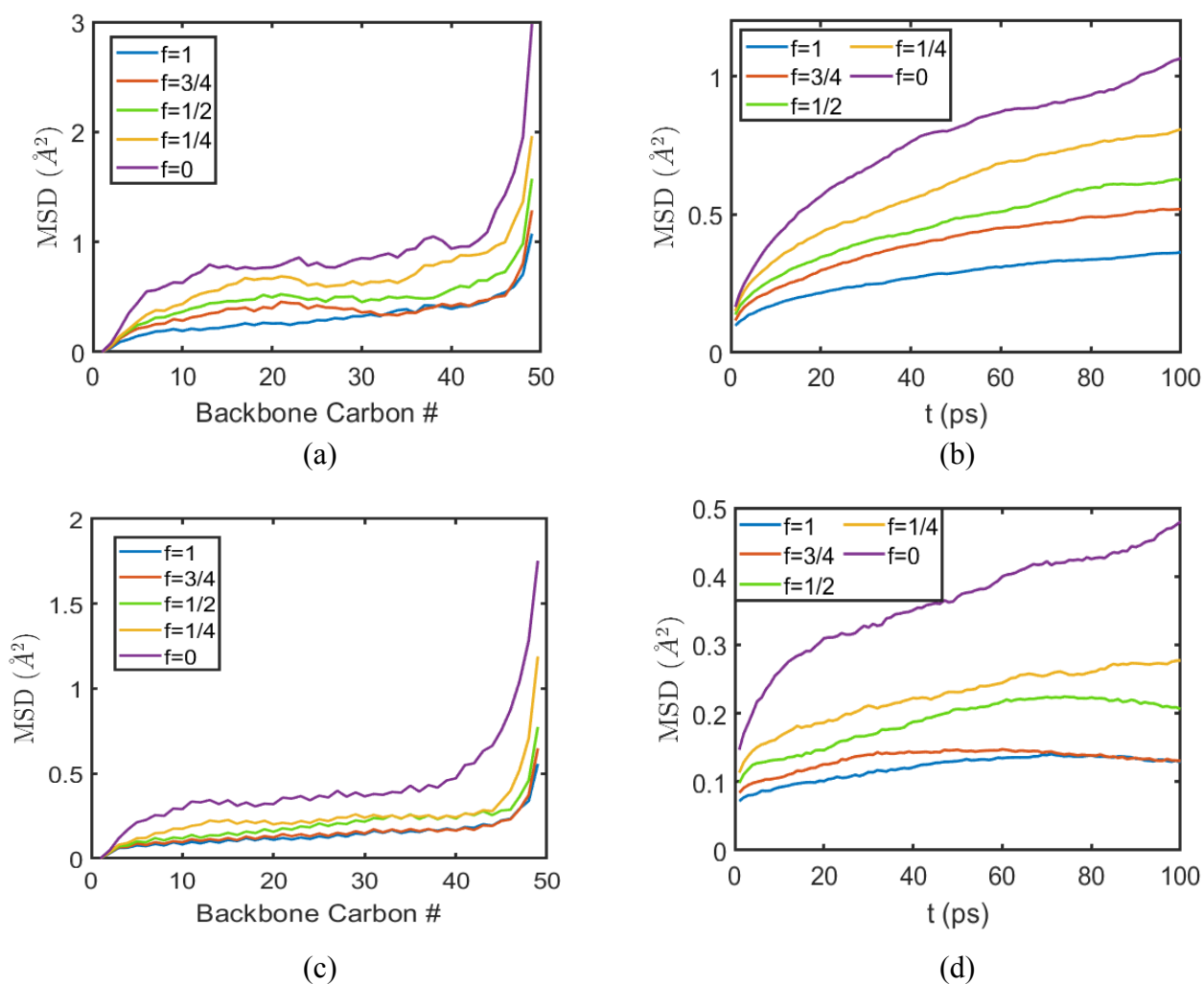
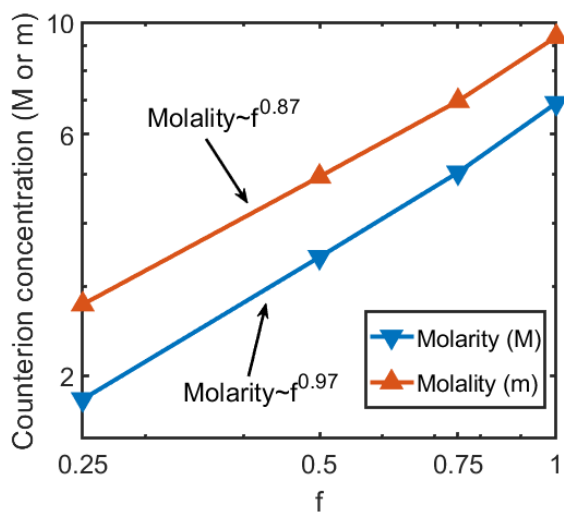


Figure S4: Stratification of the mean squared displacement (MSD) of backbone carbon atoms of the PE chains for various degrees of ionization at $t=50$ ps for (a) $\sigma_g=0.1/\sigma^2$ and (c) $\sigma_g=0.2/\sigma^2$. MSD of the middle (25^{th}) Carbon atom of the PE chains for various degrees of ionization for (b) $\sigma_g=0.1/\sigma^2$ and (d) $\sigma_g=0.2/\sigma^2$.

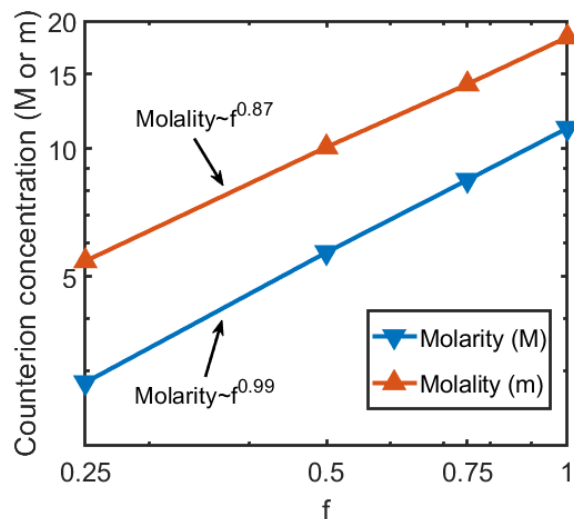
S6. Variation of Counterion Concentration

Figure S5 depicts the counterion concentration (quantified by the corresponding molarity and molality values) within the brushes for various degrees of ionization (f) and grafting densities. The total number of counterions released by the ionization of the brushes is proportional to f . We observe that almost all the counterions are trapped within the PE brush layer, irrespective of the degree of ionization and grafting density (see Figure S6). Thus, the number of moles of counterions within the brushes varies linearly with f . The increase in the volume of PE brush layer (due to an increase in brush height) with f is rather small (see Figure 2). Hence, the counterion molarity has a scaling exponent slightly less than 1 (0.97 for $\sigma_g = 0.1/\sigma^2$ and 0.99 for $\sigma_g = 0.2/\sigma^2$) with respect to the degree of ionization. The counterion molality, on the other hand, follows a scaling of $f^{0.87}$ for both the values of grafting density. Counterion molality depends on the ratio of the number of counterions to the number of water molecules i.e. the number density of counterions to that of water molecules. The number density of counterions within the brushes varies almost linearly with f (as explained previously). However, we observe an increase in the mass density (and hence the number density) of water molecules within the brushes with the degree of ionization (see section on mass density of water and Figure 9). This results in a sub-linear scaling exponent (0.87) for both $\sigma_g = 0.1/\sigma^2$ and $0.2/\sigma^2$ for counterion molality within the brushes with respect to f .

Of course, both molarity and molality of the counterions increase with the grafting density as a larger grafting density implies a larger number of charged monomers within a given volume, which will lead to a larger number of charged counterions within a fixed volume causing a larger molality and molarity.



(a)



(b)

Figure S5: Variation of counterion concentration (expressed in terms of molarity and molality) within the PE brush layer with the degree of ionization for (a) $\sigma_g=0.1/\sigma^2$ and (b) $\sigma_g=0.2/\sigma^2$. In both (a) and (b) the markers are the results from the MD simulations.

In Figure S6, we plot the transverse counterion distribution profiles $\rho_{ci}(z)$, normalized such that $\frac{1}{\sigma_g} \int_0^\infty \rho_{ci}(z) dz = N_{ci} f$, where $N_{ci} = (N - 1)/2 = 24$ is the number of counterions associated with each fully ionized PE chain.

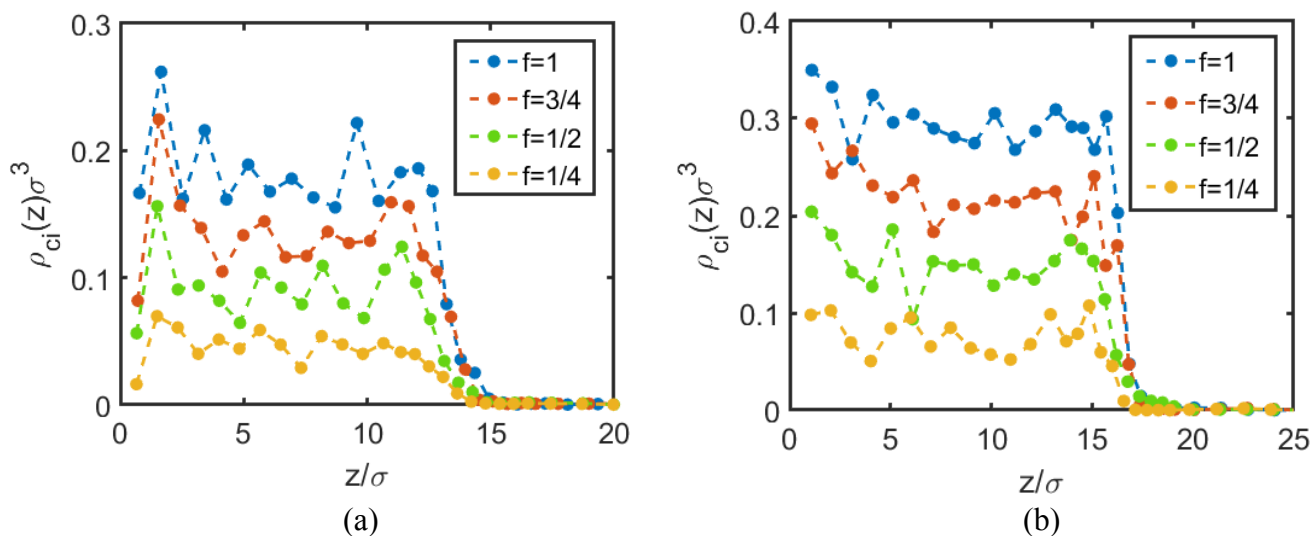


Figure S6: Transverse counterion distribution profiles $[\rho_{ci}(z)]$ for various degrees of ionization for (a) $\sigma_g = 0.1/\sigma^2$ and (b) $\sigma_g = 0.2/\sigma^2$.

We can observe that most of the counterions are present within the PE brush layer (see Table S8 for the equilibrium end-point brush heights) for all degrees of ionization and grafting densities. This is a characteristic behavior of densely grafted brushes⁷.

S7. Results for Higher Grafting Density

In this section, we provide several results discussed in the main paper for grafting density,

$$\sigma_g=0.2/\sigma^2.$$

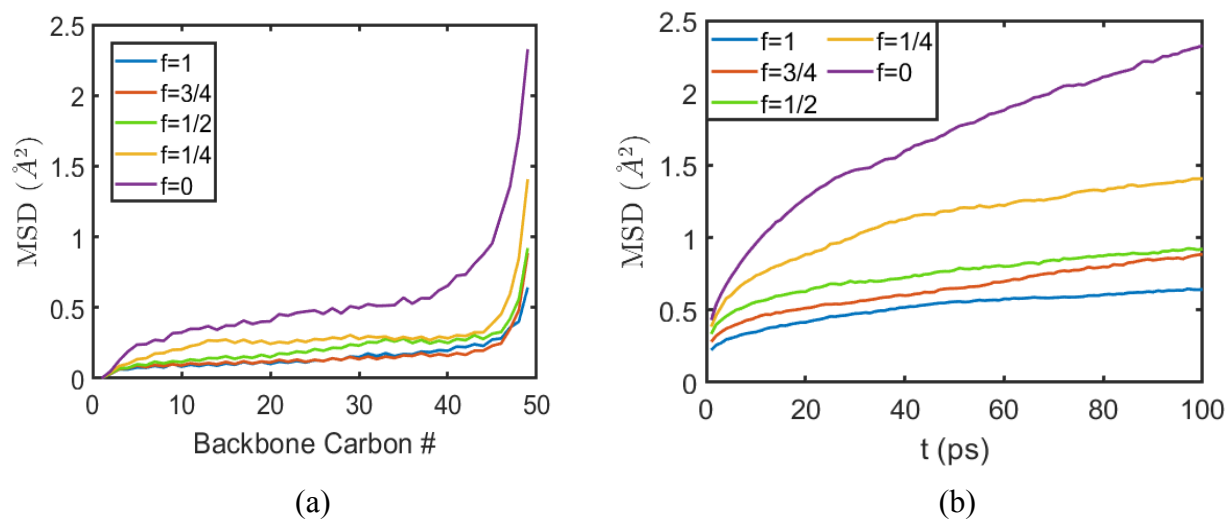


Figure S7: (a) Stratification of the mean squared displacement (MSD) of backbone carbon atoms of the PE chains for various degrees of ionization at $t=100\text{ps}$ for $\sigma_g=0.2/\sigma^2$, (b) MSD of the non-grafted terminal Carbon atom of the PE chains for various degrees of ionization for $\sigma_g=0.2/\sigma^2$.

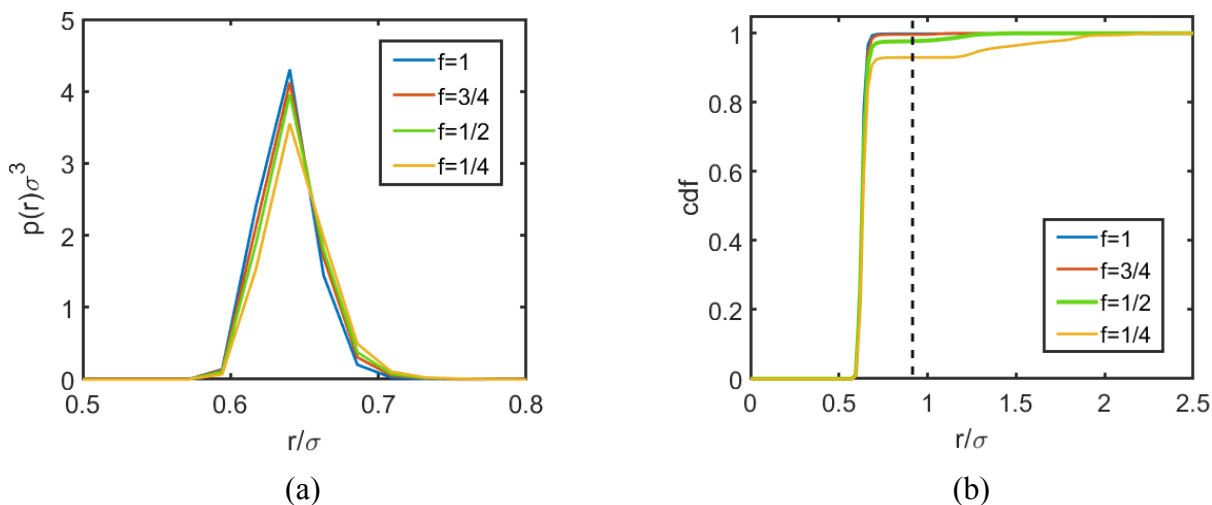


Figure S8: (a) Normalized probability distribution of finding the nearest $O_{\text{Carboxylate}}$ atom around Na^+ counterions within the PE brush layer for $\sigma_g=0.2/\sigma^2$, (b) the cumulative distribution function (cdf) for scenario depicted in (a). In (a) and (b), results are shown for different degrees of ionization.

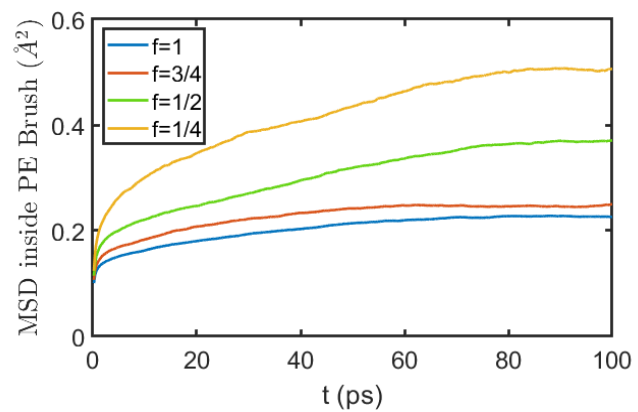


Figure S9: Mean squared displacement (MSD) of Na^+ counterions within the PE brush layer for various degrees of ionization for $\sigma_g = 0.2/\sigma^2$.

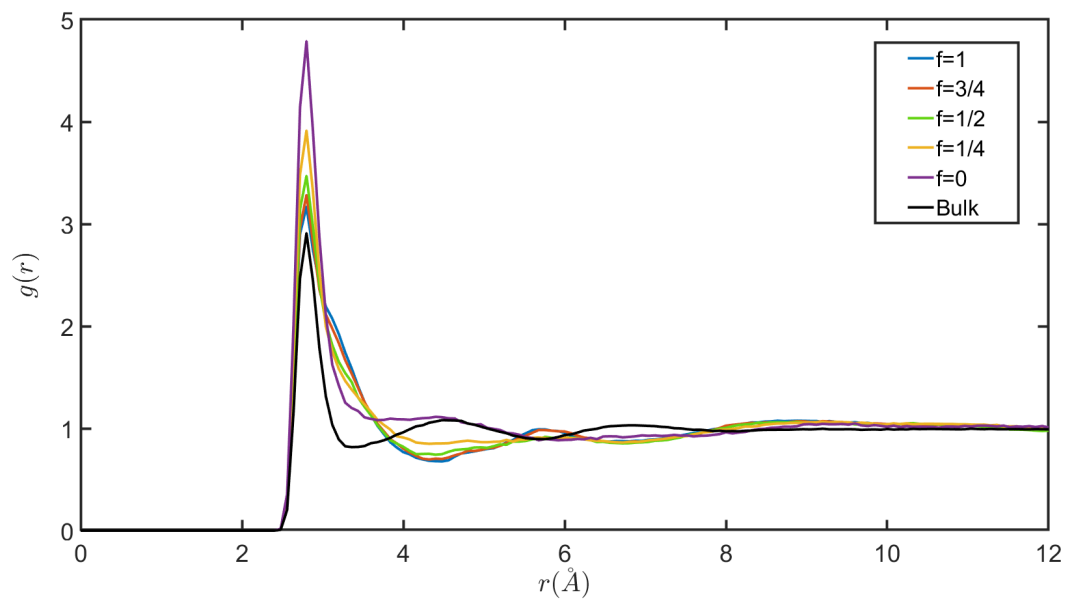


Figure S10: O_w-O_w RDF of water molecules within the PE brush layer for various degrees of ionization for $\sigma_g=0.2/\sigma^2$. Bulk O_w-O_w RDF is also provided for comparison.

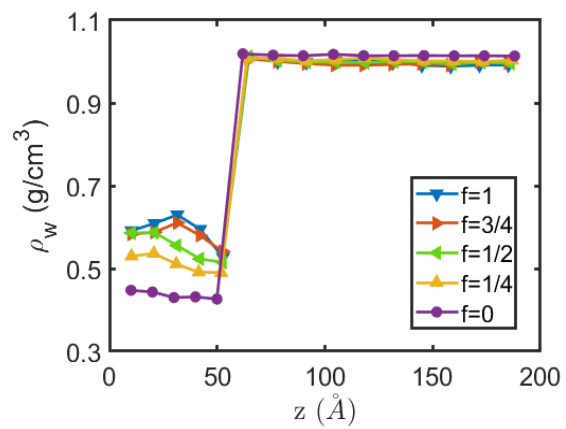


Figure S11: Transverse variation of mass density of water molecules for various degrees of ionization for $\sigma_g=0.2/\sigma^2$.

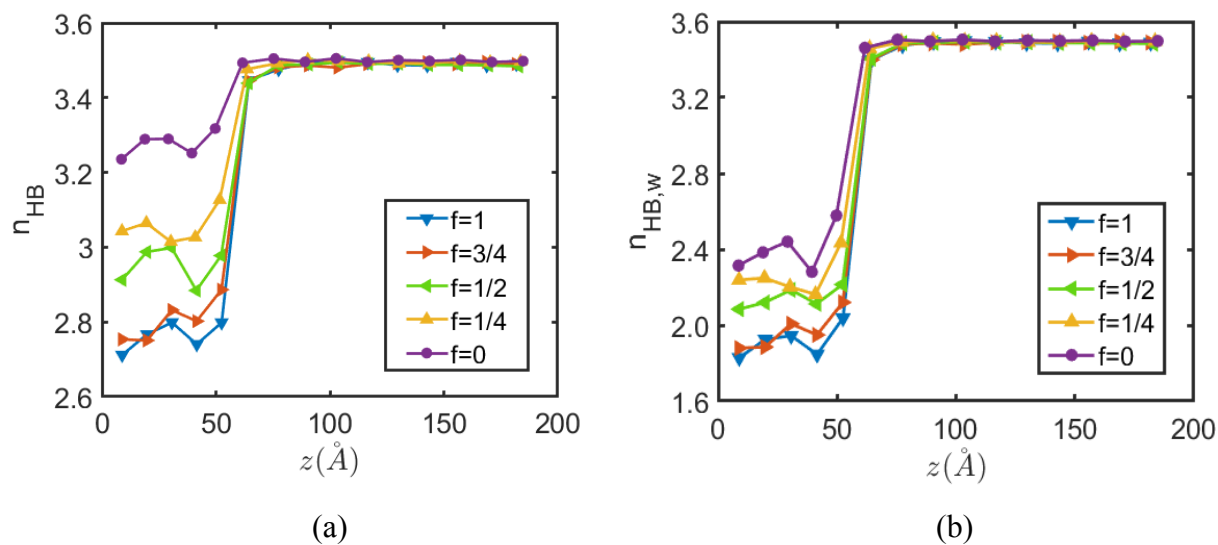


Figure S12: (a) Transverse variation in number of hydrogen bonds per water molecule n_{HB} with degree of ionization for $\sigma_g=0.2/\sigma^2$, (b) Transverse variation in number of hydrogen bonds between water molecules (per water molecule) $n_{HB,w}$ with degree of ionization for $\sigma_g=0.2/\sigma^2$.

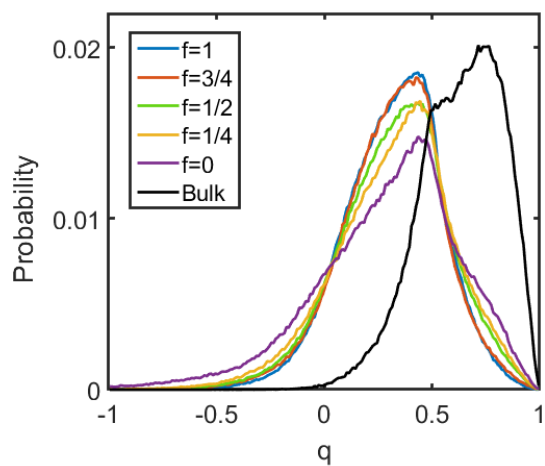


Figure S13: Probability distribution of orientational tetrahedral order parameter (q) of water molecules within the PE brushes for various degrees of ionization for $\sigma_g=0.2/\sigma^2$. Probability distribution of q for bulk SPC/E water is also provided for comparison.

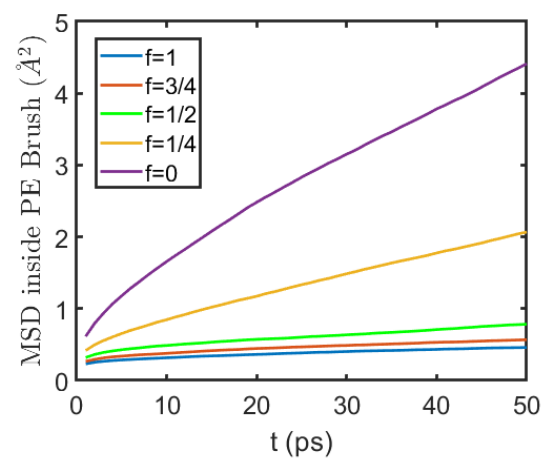


Figure S14: Mean squared displacement (MSD) of water molecules within the PE brushes for various degrees of ionization for $\sigma_g=0.2/\sigma^2$.

S8. Comparison between Solvation Structure of Condensed and Uncondensed Counterions

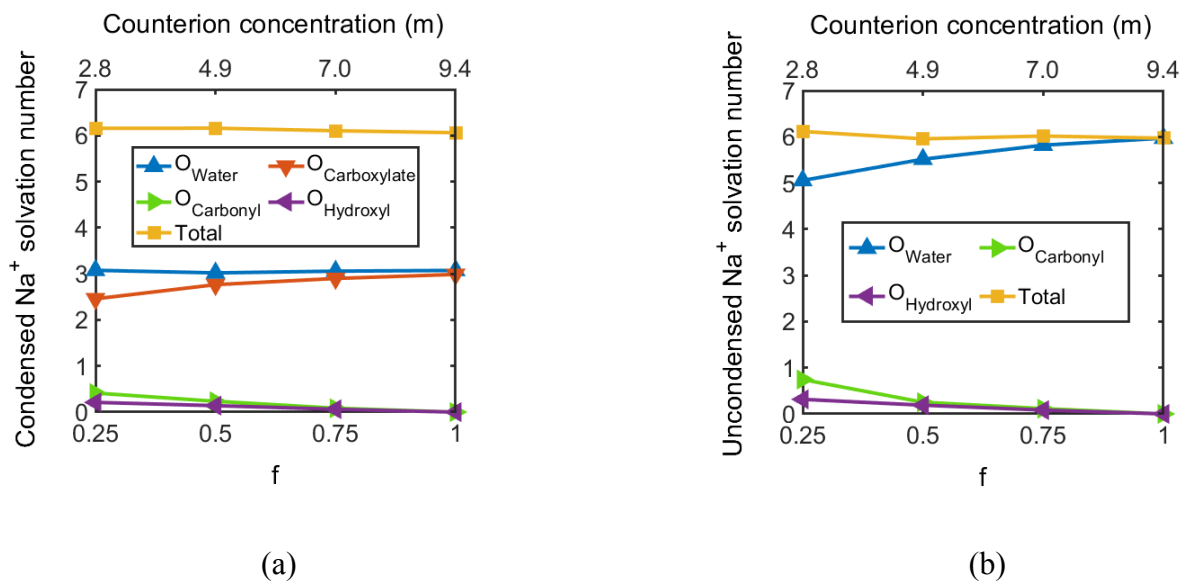


Figure S15: Variation in the solvation structure of (a) condensed Na⁺ counterions and (b) uncondensed Na⁺ counterions (within the PE brush layer) with degree of ionization for $\sigma_g=0.1/\sigma^2$.

In this section, we look into the differences in the solvation structure of condensed and uncondensed Na⁺ counterions within the brushes. Firstly, we observe that the solvation structure for the condensed counterions is very similar to the average solvation structure of Na⁺ counterions within the brushes for $\sigma_g=0.1/\sigma^2$ [compare Figures S15 and 5(a)]. This is expected as the percentage of condensed counterions is very high (> 90%) for all degrees of ionization [see Figure 4(c)]. On the other hand, the uncondensed counterions possess a distinctly different solvation structure compared to their condensed counterparts. The contribution of O_{Water} atoms in the first solvation shell of uncondensed counterions is significantly higher and approaches the bulk solvation number of aqueous Na⁺ ions (~6) as $f \rightarrow 1$.

S9. Na^+ - O_w RDF for Uncondensed Na^+ Counterions

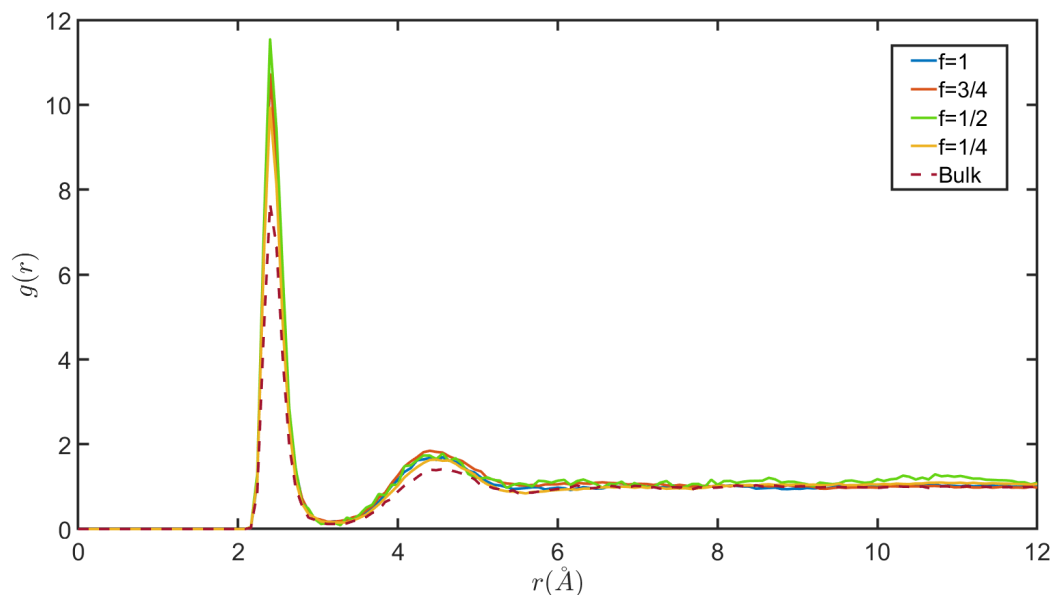


Figure S16: Variation in Na^+ - O_w RDF of uncondensed counterions within the PE brush layer with degree of ionization for $\sigma_g=0.1/\sigma^2$. Bulk Na^+ - O_w RDF is also provided for comparison (dashed line).

Figure S16 plots the Na^+ - O_w RDF of uncondensed counterions inside the brushes. We do not provide the Na^+ - O_w RDF for condensed counterions as they are very similar to the overall Na^+ - O_w RDF provided in Figure 6. We observe that the peak corresponding to the first solvation shell of Na^+ - O_w RDF for uncondensed counterions is significantly higher than that of the overall Na^+ - O_w RDF [compare Figures S16 and 6]. This is because of the significantly higher number of O_{Water} atoms inside the first solvation shell of the unbound counterions (see section S8). Moreover, there is non-monotonic variation in the first peak height with the degree of ionization for the uncondensed counterions. This is because of two competing effects. On the one hand,

there is an increase in the number of O_{water} atoms within the first solvation shell of Na^+ ions with the degree of ionization. This tends to increase the peak value of the $\text{Na}^+ - O_w$ RDF. On the other hand, the mass density of water within the brushes increases with the degree of ionization (see Figure 9). This tends to decrease the $\text{Na}^+ - O_w$ RDF peak as the RDFs are normalized with respect to the overall water density within the brushes.

S10. Comparison between $O_w - O_w$ RDF of Bound and Free Water Molecules

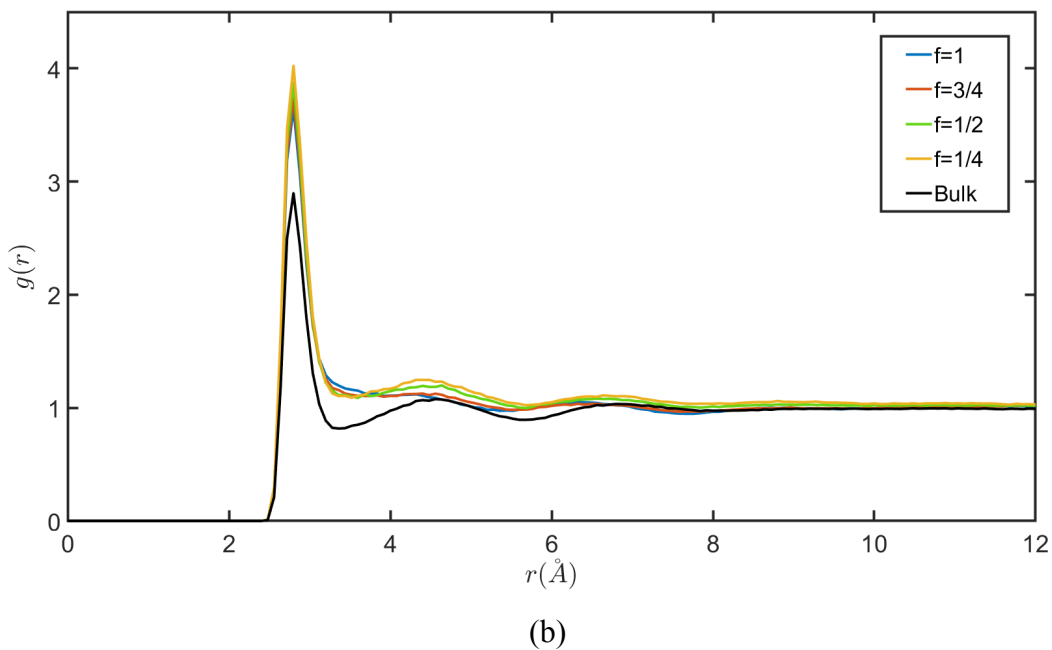
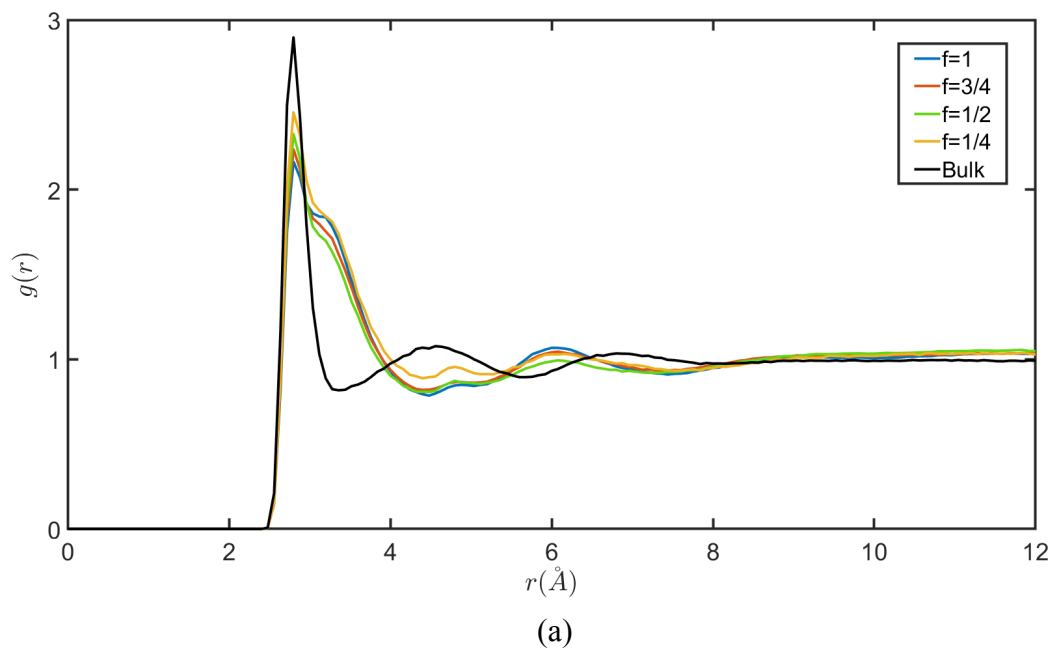


Figure S17: $O_w - O_w$ RDF of (a) bound and (b) free water molecules within the PE brush layer for various degrees of ionization for $\sigma_g = 0.1/\sigma^2$. Bulk $O_w - O_w$ RDF is also provided for comparison.

We observe that the $O_w - O_w$ RDF peak for bound water molecules is much lower than that for bulk water. This is because of the partial replacement of solvation water by Na^+ counterions. The replacement is enhanced at higher degrees of ionization (due to an increase in the counterion concentration), thereby causing a further reduction in the peak height.

The $O_w - O_w$ RDF peak for free water molecules within the brushes is much higher than the case of bulk water. This is because the overall mass density of water molecules within the brushes is lower inside the brushes as compared to bulk (the RDF is normalized with respect to the overall water density). The mass density of water within the brushes increases with degree of ionization (see Figure 9) causing a progressive decrease in the RDF peak of free water molecules.

The overall $O_w - O_w$ RDF of water molecules (within the brushes) depicted in Figure 8 reflects the weighted average of both bound and free water molecules. From Figure S17 (b), we can see that the decrease in RDF peak of free water molecules with degree of ionization is rather small. In contrast, the reduction of RDF peak with the degree of ionization for bound water molecules is much more prominent. Thus, the significant reduction in peak height with the degree of ionization observed in Figure 8 can be attributed to bound water molecules. It should also be noted that the overall $O_w - O_w$ RDF within the brushes depicts a larger peak height than bulk water as seen for the case of free water molecules.

References

1. Arnold, R. The Titration of Polymeric Acids. *J. Colloid Sci.* **1957**, 12, 549–556.
2. M. Murat; G. S. Grest. Structure of a Grafted Polymer Brush: A Molecular Dynamics Simulation. *Macromolecules* **1989**, 22, 4054–4059.
3. Ahrens, H.; Förster, S.; Helm, C. A.; Kumar, N. A.; Naji, A.; Netz, R. R.; Seidel, C. Nonlinear Osmotic Brush Regime: Experiments, Simulations and Scaling Theory. *J. Phys. Chem. B* **2004**, 108, 16870–16876.
4. Nair, A. Molecular Dynamics Simulations of Polyelectrolyte Brushes. Ph.D. Dissertation, King Abdullah University of Science and Technology, Saudi Arabia, 2006.
5. Naji, A.; Netz, R. R.; Seidel, C. Non-Linear Osmotic Brush Regime: Simulations and Mean-Field Theory. *Eur. Phys. J. E* **2003**, 12, 223–237.
6. Das, S.; Banik, M.; Chen, G.; Sinha, S.; Mukherjee, R. Polyelectrolyte Brushes: Theory, Modelling, Synthesis and Applications. *Soft Matter* **2015**, 11, 8550–8583.
7. Pincus, P. Colloid Stabilization with Grafted polyelectrolytes. *Macromolecules* **1991**, 24, 2912–2919.